

# Brazing of Mo and Nb using two active braze alloys

H.W. Chuang<sup>a</sup>, D.W. Liaw<sup>a</sup>, Y.C. Du<sup>a</sup>, R.K. Shiue<sup>b,\*</sup>

<sup>a</sup> Department of Materials Science and Engineering, National Dong Hwa University, Hualien 974, Taiwan, ROC

<sup>b</sup> Department of Materials Science and Engineering, National Taiwan University, Taipei 106, Taiwan, ROC

Received 11 May 2004; received in revised form 5 August 2004

## Abstract

The brazing of molybdenum and niobium using two active braze alloys, 63Ag–35.25Cu–1.75Ti and 68.8Ag–26.7Cu–4.5Ti, has been extensively evaluated. Both infrared and traditional vacuum furnace brazing are included in the experiment. Two active braze alloys demonstrate excellent wettability on Mo and Nb substrates, especially upon increasing the test temperature from 900 to 950 °C. For 63Ag–35.25Cu–1.75Ti braze alloy, the brazed joint primarily consists of Ag-rich and Cu-rich phases. Because the Ti is completely miscible with Mo and Nb, there is no reaction product at the interface among the braze alloy and two substrates. Accordingly, dimple-dominated fracture is extensively observed in the brazed joint. The brazed Mo/68.8Ag–26.7Cu–4.5Ti/Nb joint primarily consists of Ag-rich, Cu-rich and Nb-rich phases. A few Cu–Ti intermetallics are found in the brazed joint due to higher Ti content in the braze alloy. However, the presence of Cu–Ti intermetallic phases demonstrates little effect on the shear strength of the brazed joint. Dimple-dominated fracture is observed for the 900 °C brazed joint. The Nb-rich phase is found in both brazed joints, and its amount is increased with increasing brazing temperature and/or time. Accordingly, the growth of the Nb-rich phase is greatly inhibited during rapid infrared brazing. The coarsening of the Nb-rich phase significantly deteriorates the shear strength of the brazed Mo/68.8Ag–26.7Cu–4.5Ti/Nb joint, and finally results in cleavage fracture of the brazed joint.

© 2004 Elsevier B.V. All rights reserved.

*Keywords:* Brazing; Molybdenum; Niobium; Microstructure; Interface; Shear test

## 1. Introduction

The refractory metals include those metals that have melting points in excess of 2450 °C [1]. The most important refractory metals, from a structural standpoint, are molybdenum (Mo), tantalum (Ta), niobium (Nb) as well as tungsten (W) [1–3]. In current applications of the refractory metals in the aircraft, space, nuclear and electronic industries, joints must be of significant dimensions with properties that are adequate to meet exacting requirements of strength, ductility, corrosion resistance, etc. [3]. The welding of niobium does not present the brittleness problem associated with molybdenum. However, brazing must be considered if welding is inappropriate [4]. Brazing has been widely adopted as the way of joining assemblies made from refractory metals due to its limited effect on base-metal properties [3].

The mechanical properties of refractory metals are greatly affected by ductile-to-brittle transition behavior [1,2]. For example, the molybdenum is brittle at room temperature, and it must be brazed in a stress-free condition. The strength and ductility of refractory metals are adversely affected by the microstructural changes that occur when the recrystallization temperatures of these metals are exceeded [3]. Recrystallization temperature ranges from unalloyed Nb and Mo are 985–1150 and 1150–1200 °C, respectively [1,3]. If the maximum joint strength is required, refractory metals must be brazed at temperatures below those at which recrystallization occur. In contrast, brazing at much higher temperatures may be necessitated by service requirements, and some decrease in joint properties can be expected [3].

Refractory metals can be brazed with gold, palladium, platinum, reactive metals and nickel-based braze alloys for high-temperature applications [3,4–10]. In contrast, copper and silver-based braze alloys can be applied in brazing refractory metals for low-temperature service. The successful

\* Corresponding author. Tel.: +886 2 2702 3069; fax: +886 2 2363 4562.  
E-mail address: rkshiue@ccms.ntu.edu.tw (R.K. Shiue).

Table 1  
Summary of the process variables used in the experiment

Composition of braze alloys (wt.%)	63Ag–35.25Cu–1.75Ti	68.8Ag–26.7Cu–4.5Ti
Solidus/liquidus temperature (°C)	780/815	830/850
Furnace brazing temperature (°C)	900, 950	900, 950
Furnace brazing time (s)	600, 1200, 1800	600, 1200, 1800
Infrared brazing temperature (°C)	900, 950	900, 950
Infrared brazing time (s)	180, 300	180, 300

brazing of Ti–6Al–4V and molybdenum alloy using three silver-based brazes has been accomplished in previous studies [11–13]. The eutectic composition of Ag and Cu in weight percent is 72Ag–28Cu, and it exhibits a low melting point (780 °C) as well as excellent fluidity upon melting [3,5]. However, the molybdenum alloy is not effectively wetted by the molten braze even upon increasing the temperature up to 900 °C [11]. It has been reported that active-metal modification, e.g., titanium additions, of the silver–copper eutectic braze may be useful for brazing refractory metals [4]. Two active braze alloys with the chemical composition of 63Ag–35.25Cu–1.75Ti and 68.8Ag–26.7Cu–4.5Ti in weight percent are chosen in order to improve the wettability of the molten braze on both refractory substrates.

The development of high-intensity quartz lamps and the availability of suitable reflectors have made infrared heating an important source of heat for brazing [6]. Compared with the conventional vacuum furnace brazing, infrared vacuum brazing is characterized by a very rapid thermal cycle with the heating rate as high as 3000 °C/min [14–17]. Decreasing the brazing temperature and/or time is always recommended with the advantages of decreased interfacial reactions, decreased erosion of substrates and minimum loss of base-metal properties [3,5,11]. Therefore, infrared brazing of Mo and Nb metals is also included in the experiment in addition to conventional furnace brazing. This investigation is concentrated on vacuum brazing of molybdenum and niobium below their recrystallization temperatures. Two active braze alloys are selected as the brazing filler metals. Wettability of various brazes on both substrates, microstructural evolution and shear strength of the brazed joint have been extensively evaluated.

## 2. Experimental

The base metals used in the test were pure molybdenum and niobium disks with the dimension of 25 mm in diameter and 3 mm in thickness. Both substrates were polished with SiC papers up to grit 1200, and subsequently cleaned using an ultrasonic bath with acetone as the fluid prior to brazing. 63Ag–35.25Cu–1.75Ti and 68.8Ag–26.7Cu–4.5Ti in weight percent were selected as the brazing filler metals. They were in the form of foil with a thickness of 50 µm and a width of 50 mm.

Sessile drop tests were performed using a conventional vacuum furnace with various temperatures for 0–2400 s

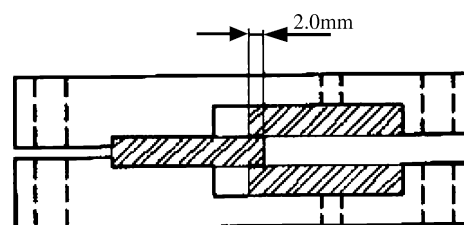


Fig. 1. Schematic diagram of the shear test specimen [17].

[18,19]. The heating rate of the vacuum furnace was maintained at 30 °C/min, and the average cooling rate was approximately the same as heating rate. The braze alloy with near spherical shape used in the sessile drop test was prepared from the braze alloy foils by vacuum arc remelting (VAR) with an operation voltage of 60 V and a current 130–150 A. The weight of each spherical ball was approximately 0.12 g [18,19]. The spherical ball was placed on the molybdenum and niobium substrates, respectively. The image of the molten braze on the substrate was recorded simultaneously using an Olympus C-5050 digital camera during the wetting angle measurement.

Both furnace brazing and infrared brazing were performed in the experiment with a vacuum of  $5 \times 10^{-5}$  mbar at various specified temperatures. The heating rate of infrared furnace was kept at 600 °C/min throughout the experiment. Additionally, all brazed specimens were preheated at 600 °C for 600 s before the brazing temperature was attained. Table 1 summarizes all brazing process variables used in the study.

Specimen was cut using a low-speed diamond saw, and subsequently processed by standard metallographic procedure prior to inspection. The cross-section of the brazed specimens was examined using a Hitachi 3500H scanning electron microscope (SEM) with an accelerating voltage of 15 kV. Quantitative chemical analysis was performed using a JEOL JXL-8900R electron probe microanalyzer (EPMA) with an operation voltage of 20 kV and spot size of 1 µm.

Shear tests were performed in order to evaluate the bonding strength of selected (infrared) brazed specimens [15,17]. Fig. 1 shows the shear test specimen used in this experiment [17]. The middle shaded area is the Nb substrate and two Mo substrates are the outer shaded areas next to the Nb. The outer part of the layout is the graphite fixture used in the infrared brazing. Additionally, two bold black lines with 2.0 mm wide in the middle of the graph indicate the location of braze alloy, and the specimen is sandwiched between two graphite

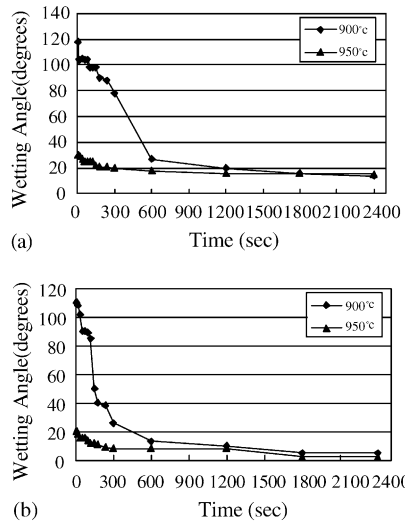


Fig. 2. The sessile drop tests of 63Ag–35.25Cu–1.75Ti braze alloy on (a) Mo and (b) Nb substrates at various temperatures for 0–2400 s.

plates. The shear test was performed by the Shimadzu AG-10 universal testing machine to evaluate the bonding strength of the infrared brazed joint. A Shimadzu AG-10 universal testing machine with a constant crosshead speed of 0.5 mm/min compressed the brazed specimens. The fractured surfaces after shear tests were examined using the SEM.

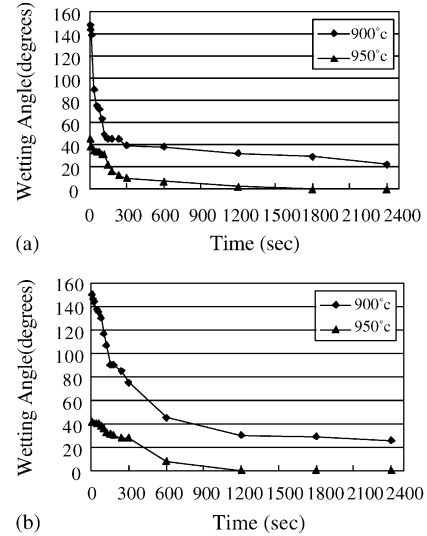
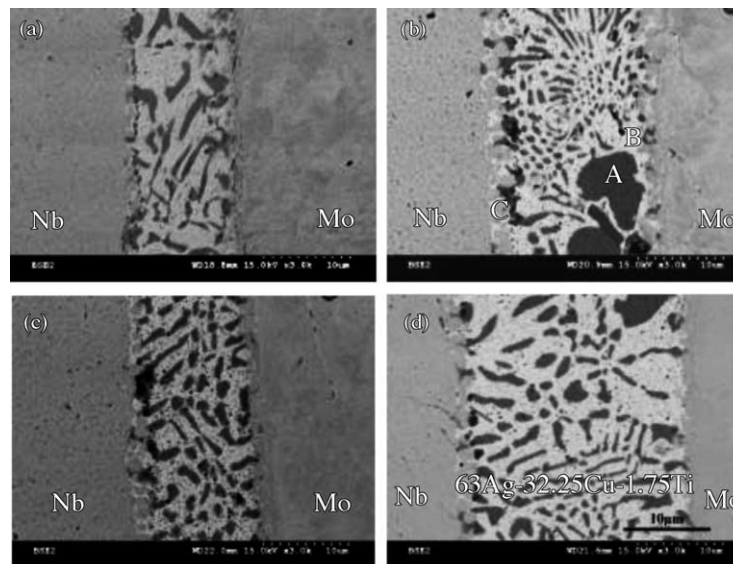


Fig. 3. The sessile drop tests of 68.8Ag–26.7Cu–4.5Ti braze alloy on (a) Mo and (b) Nb substrates at various temperatures for 0–2400 s.

### 3. Results and discussion

#### 3.1. Sessile drop tests of two active brazes on Mo and Nb substrates

Based on the previous study, the wettability of Ag–Cu eutectic braze (72Ag–28Cu, wt.%) cannot effectively wet the molybdenum alloy at 900 °C, and the wetting angle of molten



Location (phase), at%	Nb	Mo	Ag	Cu	Ti
A (Cu-rich)	0.1	0.1	5.8	88.5	5.5
B (Ag-rich)	0.2	0.3	88.7	10.7	0.1
C (Nb-rich)	82.0	2.2	0.4	5.5	10.0

Fig. 4. . The SEM BEIs of the infrared brazed 63Ag–35.25Cu–1.75Ti specimen at (a) 900 °C × 180 s, (b) 900 °C × 300 s, (c) 950 °C × 180 s and (d) 950 °C × 300 s.



and Cu-rich phases alloyed with Ti, Cu and Ag, respectively.

The molten braze may react with both substrates, and both substrates are dissolved into the molten braze during (infrared) brazing. According to the related binary alloy phase diagrams, the solubility of both Mo and Nb metals in liquid Ag and/or Cu matrix is extremely limited [20]. Additionally, no intermediate compound has been reported for the Ag–Mo, Ag–Nb, Cu–Mo and Cu–Nb systems [20]. In contrast, Mo, Nb and  $\beta$ Ti are completely miscible, and there is no intermediate compound in Nb–Ti and Mo–Ti binary phase diagrams [20]. Consequently, only Ti in the active braze alloy can be dissolved into both substrates due to complete miscibility

among Mo, Nb and  $\beta$ Ti [20,21]. Accordingly, the Ti content in the molten braze is depleted during (infrared) brazing.

Fig. 5 shows the liquidus projection of Ag–Cu–Ti ternary alloy phase diagram in atomic percent [21]. The chemical composition of the active braze alloy in atomic percent is 49.7% Ag, 47.2% Cu and 3.1% Ti as marked by point A in Fig. 5. Since the liquidus temperature of 63Ag–35.25Cu–1.75Ti is 815 °C, the braze alloy forms a homogeneous liquid at the brazing temperatures of 900 and 950 °C, respectively. If the cooling path of the molten braze follows the liquidus projection of Ag–Cu–Ti phase diagram, point A in Fig. 5 will move towards to U<sub>6</sub> and U<sub>7</sub>. The

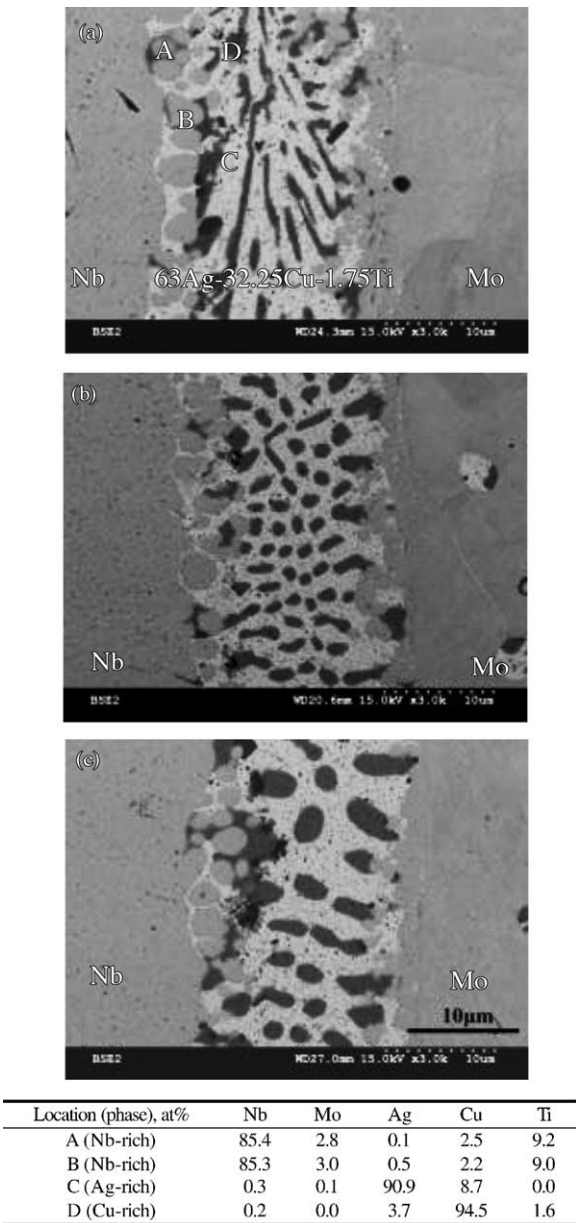


Fig. 6. The SEM BEIs and EPMA chemical analyses of the furnace brazed 63Ag–35.25Cu–1.75Ti specimens at 900 °C for (a) 600 s, (b) 1200 s and (c) 1800 s.

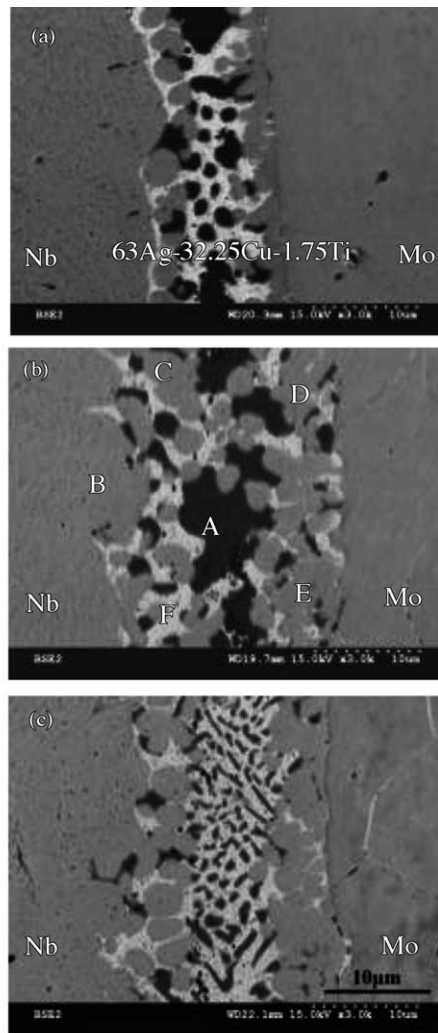
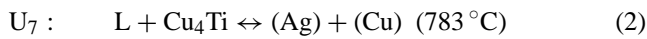
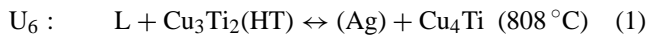


Fig. 7. The SEM BEIs and EPMA chemical analyses of the furnace brazed 63Ag–35.25Cu–1.75Ti specimens at 950 °C for (a) 600 s, (b) 1200 s and (c) 1800 s.

Table 2  
Shear strengths of various brazed specimens

Braze alloy (wt.%)	Brazing type	Temperature (°C)	Time (s)	Shear strength (MPa)	Average shear strength (MPa)	Standard deviation (MPa)
63Ag–35.25Cu–1.75Ti	Infrared	900	180	186.9	201.7	14.8
			180	216.5		
	Furnace	900	1200	191.4	186.0	5.4
			1200	180.6		
			1200	182.9		
68.8Ag–26.7Cu–4.5Ti	Infrared	900	180	217.8	213.9	3.9
			180	210.0		
	Furnace	900	1200	154.5	164.4	1.0
			1200	174.4		
Furnace	950	1200	97.8	92.7	5.1	
		1200	87.6			

reaction scheme of  $U_6$  and  $U_7$  are listed below [21,22]:



Therefore, the microstructure of the brazed joint is mainly comprised of Ag-rich and Cu-rich phases. This is consistent with the experimental observations.

Fig. 6 shows the SEM BEIs and EPMA chemical analyses of the furnace brazed 63Ag–35.25Cu–1.75Ti specimens

at 900 °C for 600, 1200 and 1800 s, respectively. Similar to the aforementioned results, the brazed joint is primarily consists of Ag-rich and Cu-rich phases. Additionally, the spherical Nb-rich phase mainly alloyed with Ti is also found at the interface between the braze alloy and Nb substrate. As discussed earlier, the addition of 1.75 wt.% titanium into the Ag–Cu eutectic braze alloy can significantly improve wettability of the molten braze on Nb substrate.

Fig. 7 displays the SEM images and EPMA chemical analyses of the furnace brazed 63Ag–35.25Cu–1.75Ti

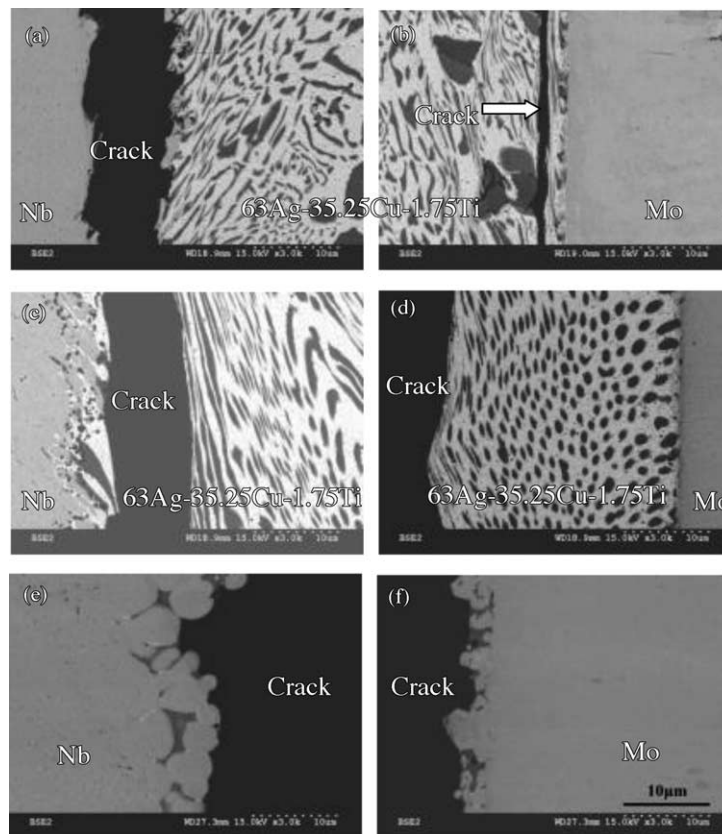


Fig. 8. SEM BEIs displaying the cross-section of brazed Mo/63Ag–35.25Cu–1.75Ti/Nb joints after shear test: (a and b) infrared brazing, 900 °C × 180 s; (c and d) furnace brazing, 900 °C × 1200 s; (e and f) furnace brazing, 950 °C × 1200 s.

specimens at 950 °C for various time periods. The brazed joint is composed of Ag-rich and Cu-rich, Nb-rich and (Mo, Nb) phases. Compared with infrared brazing, the amount of interfacial phase(s), e.g., Nb-rich and (Mo, Nb), is significantly increased for traditional furnace brazing due to its slow thermal history. It is reasonable to conclude that the interfacial reaction among the molten braze and both substrates are greatly enhanced with increasing brazing temperature and/or time as compared among Figs. 4, 6 and 7.

Table 2 summarizes shear strengths of all brazed specimens for various brazing conditions. For Mo/63Ag–35.25Cu–1.75Ti/Nb joint, the specimen infrared brazed at 900 °C for 180 s demonstrates the highest average shear strength up to 201.7 MPa. Increasing brazing temperature and/or time slightly deteriorates the shear strength of the brazed joint. The cross-sections of above fractured specimens are mounted in an epoxy, and examined by an SEM in order to proceed failure analysis of fractured joints.

Fig. 8 shows the cross-section of Mo/63Ag–35.25Cu–1.75Ti/Nb joint for various brazing conditions after shear testing. It is clear that failure of the brazed joint occurred in the braze alloy close to the interface between the braze alloy and substrate. Additionally, significant distortion of the eutectic Ag–Cu brazed alloy due to high flow stress during the shear test is also widely observed as illustrated in Fig. 8(a)–(d). The brazed joint mainly consists of Ag-rich and Cu-rich phases. It is reasonable to conclude that the eutectic microstructure with finer grain size demonstrates higher strength. The infrared brazed specimens have the finest microstructure. Accordingly, they show the higher shear strength among all brazed Mo/63Ag–35.25Cu–1.75Ti/Nb joints. Fig. 9 shows fractographs of Mo/63Ag–35.25Cu–1.75Ti/Nb joints after shear testing. Accordingly, dimple-dominated fracture is extensively observed for most fractured surfaces.

### 3.3. Evaluation of (infrared) brazed Mo/68.8Ag–26.7Cu–4.5Ti/Nb joints

Fig. 10 displays the SEM BEIs of the infrared brazed 68.8Ag–26.7Cu–4.5Ti specimens for various brazing conditions. Similar to the microstructure of brazed 63Ag–35.25Cu–1.75Ti joint, the brazed 68.8Ag–26.7Cu–4.5Ti joint is mainly comprised of Ag-rich (marked by A), Cu-rich (marked by B) and Nb-rich phases (marked by E and G). However, the existence of TiCu (marked by C) and Ti<sub>3</sub>Cu<sub>4</sub> (marked by F and H) in the infrared brazed 68.8Ag–26.7Cu–4.5Ti joint is very different from those in brazed 63Ag–35.25Cu–1.75Ti joint. The formation of TiCu and Ti<sub>3</sub>Cu<sub>4</sub> can be explained by the Ag–Cu–Ti ternary alloy phase diagram [21,22].

The chemical composition of the active braze alloy in atomic percent is 55.3% Ag, 36.5% Cu and 8.2% Ti as marked by point B in Fig. 5. There is a huge miscibility gap among the liquids as demonstrated in Fig. 5, and the chemical composition of 68.8Ag–26.7Cu–4.5Ti braze alloy is located inside the huge miscibility gap. Consequently, it is expected that the

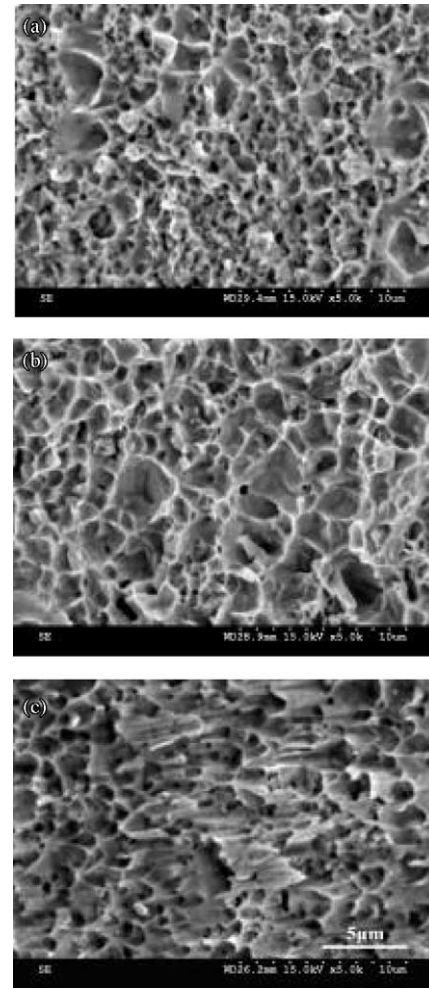


Fig. 9. SEM fractographs of the brazed 63Ag–35.25Cu–1.75Ti specimens after the shear test: (a) infrared brazing, 900 °C × 180 s; (b) furnace brazing, 900 °C × 1200 s; (c) furnace brazing, 950 °C × 1200 s.

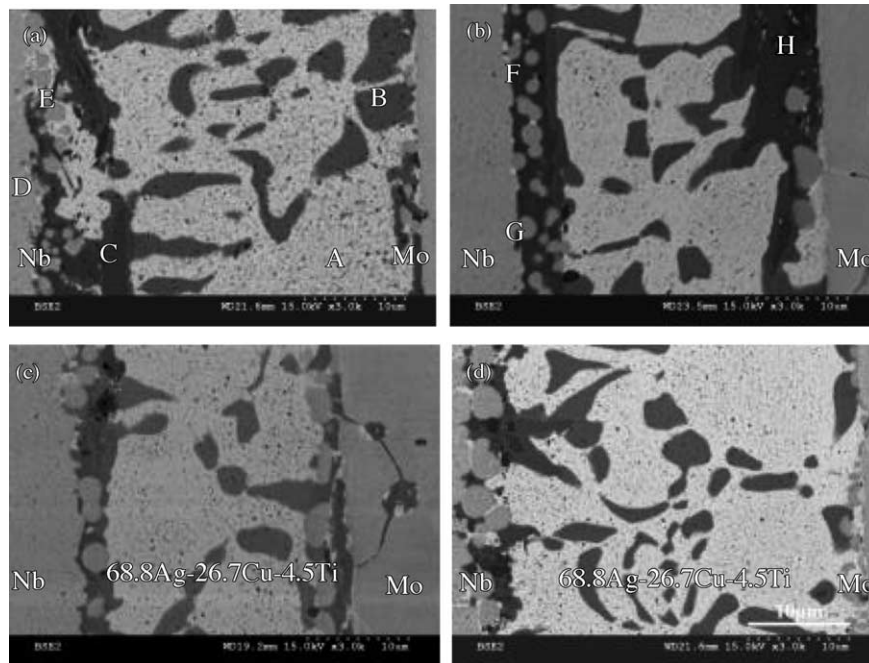
molten braze tends to separate into two liquids during brazing. One is rich in Ag, and the other liquid is rich in both Cu and Ti [21]. For instance, the reaction scheme of two immiscible liquids,  $L_1''$  and  $L_2''$ , at 900 °C is illustrated as below [21,22]:



According to Fig. 5, the  $L_1''$  liquid is rich in Cu and Ti. It is expected that the existence of  $L_1''$  liquid significantly promotes wettability of the molten braze on both substrates due to the presence of active ingredient, titanium. Complete miscibility among Mo, Nb and Ti is achieved from consulting the Mo–Nb–Ti ternary alloy phase diagram [21]. If the  $L_1''$  liquid follows the cooling path towards to point  $c_1$ , and its reaction is shown below [21,22]:



Both CuTi and Cu<sub>4</sub>Ti<sub>3</sub> phases are observed at the interface between the braze alloy and the substrate as illustrated Fig. 10



Location (phase), at%	Nb	Mo	Ag	Cu	Ti
A (Ag-rich)	0.4	0.0	86.8	12.7	0.1
B (Cu-rich)	0.2	0.0	4.2	92.0	3.6
C (TiCu)	6.3	0.1	1.9	46.6	45.1
D (Nb-rich)	96.6	0.7	0.1	2.3	0.2
E (Nb-rich)	68.5	0.2	5.2	6.8	19.3
F (Ti <sub>3</sub> Cu <sub>4</sub> )	1.9	0.1	1.7	53.7	42.5
G (Nb-rich)	74.9	0.5	0.3	4.7	19.6
H (Ti <sub>3</sub> Cu <sub>4</sub> )	2.1	0.1	1.0	54.8	42.0

Fig. 10. The SEM BEIs and EPMA chemical analyses of the infrared brazed 68.8Ag–26.7Cu–4.5Ti specimen at (a) 900 °C × 180 s, (b) 900 °C × 300 s, (c) 950 °C × 180 s and (d) 950 °C × 300 s.

(marked by C, F and H). Therefore, it is in accordance with the experimental observations.

On the other hand, the  $L_2'$  liquid is rich in silver and copper as demonstrated in Fig. 5. Consequently, it has little contribution for the molten braze to wet both substrates due to very limited solubility of Mo and Nb in molten Ag and/or Cu [20]. Both Ag-rich matrix and Cu-rich phases are formed in the joint after solidification of the  $L_2'$  liquid during brazing as displayed in Fig. 10.

Fig. 11 displays the SEM images and EPMA chemical analyses of the furnace brazed 68.8Ag–26.7Cu–4.5Ti specimens at 900 °C for various brazing time. Similar to the aforementioned result, the furnace brazed joint is primarily consists of Ag-rich (marked by D and E), Cu-rich (marked by H) and Nb-rich (marked by B, C, F and G) phases. Additionally, Ti<sub>3</sub>Cu<sub>4</sub> (marked by I) is also observed in the furnace brazed joint. It is also noted that the Nb-rich phase close to the Mo substrate is alloyed with high content of Mo as marked by F and G in Fig. 11. The amount of Nb-rich phase is increased with increasing brazing time at 900 °C.

Fig. 12 shows the SEM BEIs and EPMA chemical analyses of the furnace brazed 68.8Ag–26.7Cu–4.5Ti specimens

at 950 °C for various brazing time periods. Similar to the joint brazed at 900 °C, the joint brazed at 950 °C consists of Ag-rich, Cu-rich and Nb-rich phases. The amount of Nb-rich phase in the brazed joint is greatly increased with increasing brazing temperature. Accordingly, the wettability of the molten braze on both substrates is further improved as the temperature increased from 900 to 950 °C. Additionally, a phase mainly alloyed with Mo–Cu–Ti is observed along the grain boundary of Mo substrate as marked by E in Fig. 12(b).

Table 2 shows shear strengths of 68.8Ag–26.7Cu–4.5Ti brazed joint for various brazing conditions. The infrared brazed specimen at 900 °C for 180 s exhibits the highest average shear strength of 213.9 MPa. Increasing brazing temperature and/or time significantly deteriorates shear strength of the brazed joint. According to Figs. 10(a), 11(d) and 12(c), the amount of Nb-rich phase is increased with brazing time and/or temperature, especially for the specimen brazed at 950 °C exceeding 1200 s. The Nb-rich phase becomes the dominant phase in the brazed joint as illustrated in Fig. 12(c) and (d). It is reasonable to deduce that the significant loss of shear strength for the brazed joint at 950 °C is caused by excessive growth of the Nb-rich phase.

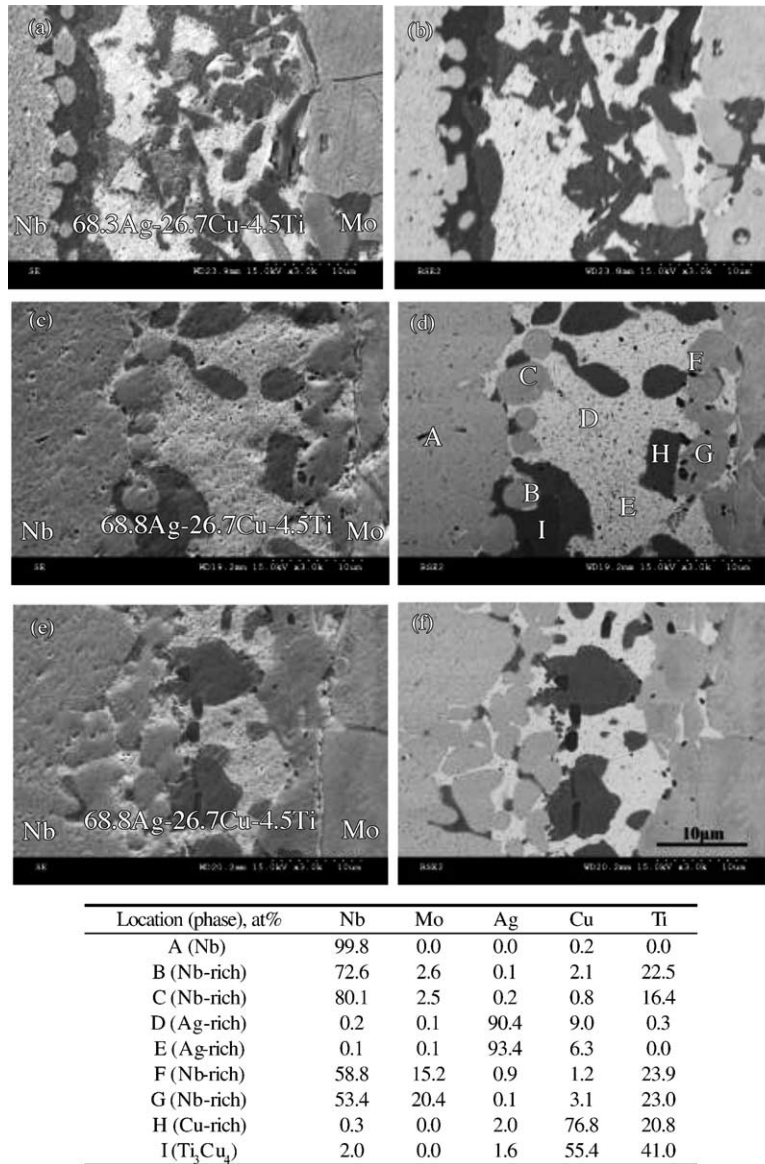


Fig. 11. The SEM images and EPMA chemical analyses of the furnace brazed 68.8Ag–26.7Cu–4.5Ti specimens at 900 °C: (a) SEI, (b) BEI for 600 s; (c) SEI, (d) BEI for 1200 s; (e) SEI, (f) BEI for 1800 s.

Fig. 13 shows the cross-section of brazed Mo/68.8Ag–26.7Cu–4.5Ti/Nb joint after shear test. The fracture of infrared brazed specimen with the highest shear strength is located at the interface close to the Nb substrate. For specimen furnace brazed at 900 °C is fractured at the interface between the braze and Nb substrate. The distortion of braze alloy due to huge plastic deformation is observed in Fig. 14(b) and (c). Different from the above cases, the specimen furnace brazed at 950 °C is fractured at the braze alloy, and very limited plastic deformation is found in Fig. 13(d). It is clear that the prominent Nb-rich phase is detrimental to shear strength of the brazed joint.

Fig. 14 displays SEM fractographs of the brazed Mo/68.8Ag–26.7Cu–4.5Ti/Nb specimens after the shear test. Dimple-dominated fracture is observed for specimen brazed

at 900 °C as illustrated in Fig. 14(a) and (b). In contrast, the fractograph demonstrates brittle fracture for the specimen furnace brazed at 950 °C (Fig. 14(c)). The dominated spherical Nb-rich phase is responsible for the inherent brittleness of the brazed joint.

### 3.4. Discussion of experimental results

Based on the previous study, Ti–6Al–4V and molybdenum are successfully brazed using the Ag–Cu eutectic braze alloy [11]. The microstructure of brazed joint is mainly comprised of Ag-rich matrix and interfacial Ti<sub>2</sub>Cu, TiCu and Ti<sub>3</sub>Cu<sub>4</sub> reaction layers. The Ti–6Al–4V substrate readily reacts with the molten braze, and forms reaction layers [11]. The thickness of Cu–Ti interfacial layer is increased with increasing

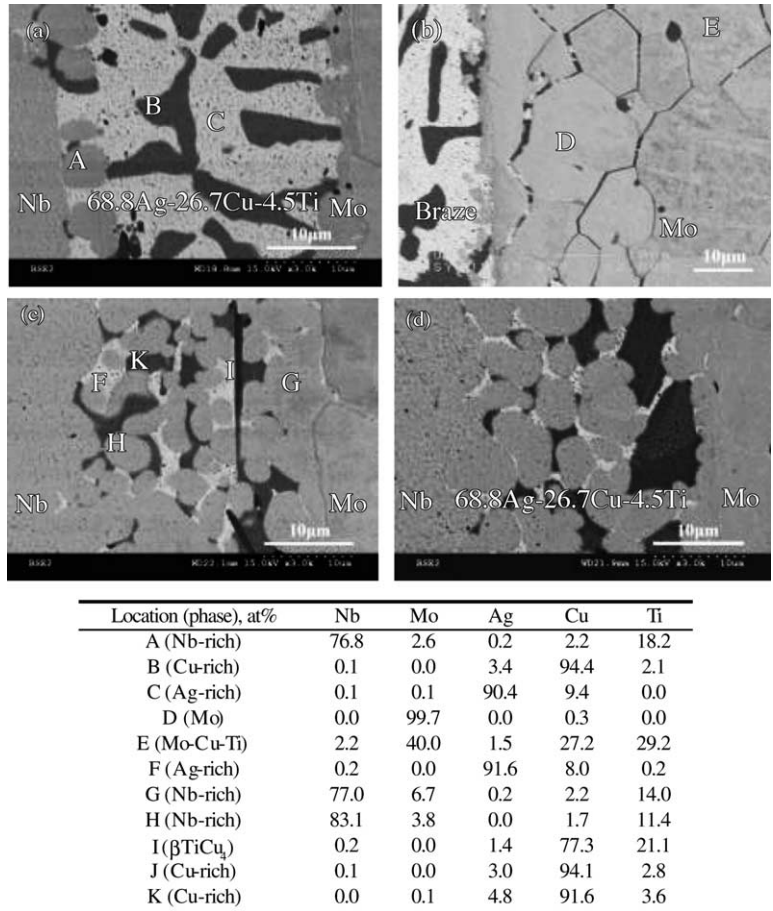


Fig. 12. The SEM BEIs and EPMA chemical analyses of the furnace brazed 68.8Ag–26.7Cu–4.5Ti specimens at 950 °C for (a, b) 600 s, (c) 1200 s and (d) 1800 s.

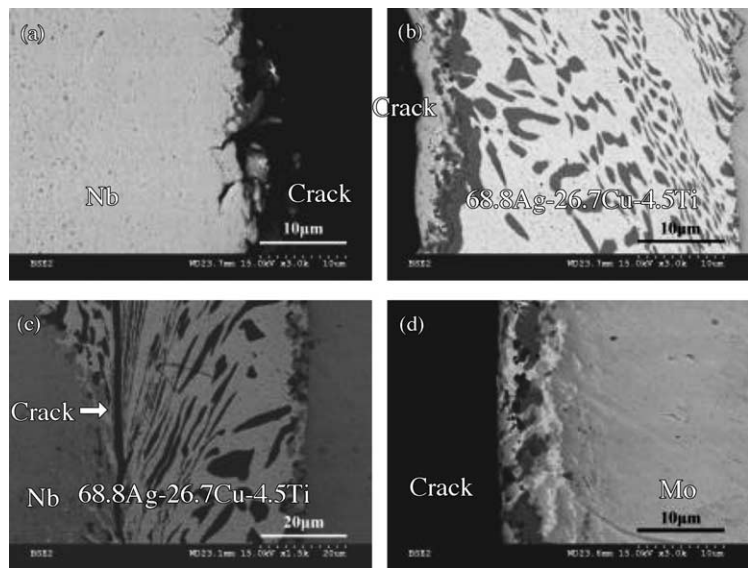


Fig. 13. SEM BEIs displaying the cross-section of brazed Mo/68.8Ag–26.7Cu–4.5Ti/Nb joint after shear test: (a, b) infrared brazing, 900 °C × 180 s; (c) furnace brazing, 900 °C × 1200 s; (d) furnace brazing, 950 °C × 1200 s.

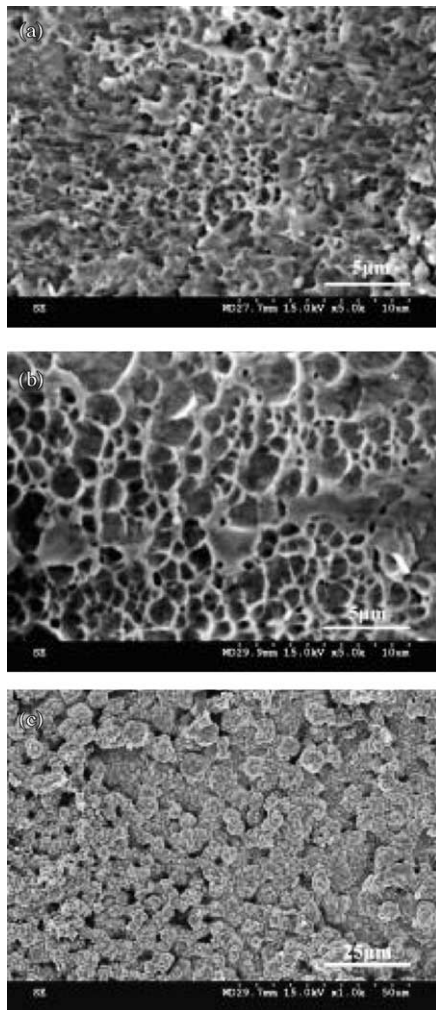


Fig. 14. SEM fractographs of the brazed Mo/68.8Ag–26.7Cu–4.5Ti/Nb specimens after the shear test: (a) infrared brazing, 900 °C × 180 s; (b) furnace brazing, 900 °C × 1200 s; (c) furnace brazing, 950 °C × 1200 s.

brazing temperature and/or time. Additionally, it is also reported that the growth of Cu–Ti intermetallics is usually detrimental to the bonding strength of the brazed joint, and the cleavage-dominated fracture is widely observed in the brazed joint [22].

In contrast, there is no continuous interfacial reaction layer observed in the brazed Mo/63Ag–35.25Cu–1.75Ti/Nb joint. Because the Ti is completely miscible with Mo and Nb, there is no reaction product at the interface among the braze alloy and two substrates. From the viewpoint of brazing technology, it is preferred that the brazed joint is free of any brittle intermetallic compound. Accordingly, dimple-dominated fracture is extensively observed in the brazed joint as illustrated in Fig. 9.

For the brazed 68.8Ag–26.7Cu–4.5Ti joint, a few Cu–Ti intermetallics are found in the brazed joint due to higher Ti content in the braze alloy. However, the growth of Cu–Ti intermetallics is not prominent during brazing due to depletion of Ti content from the molten braze. The presence of

Cu–Ti intermetallic phase demonstrates little effect on the shear strength of the brazed joint. Dimple-dominated fracture is observed for the 900 °C brazed specimen. Additionally, the Nb-rich phase is found in the brazed joint. The amount of Nb-rich phase is increased with increasing brazing temperature and/or time. The coarsening of the Nb-rich phase deteriorates the shear strength of the joint, and finally results in cleavage fracture of the brazed joint.

#### 4. Conclusions

Evaluation of the (infrared) brazed molybdenum and niobium joint using two active braze alloys has been extensively studied. The primary conclusions are summarized as below:

1. Both active braze alloys exhibit excellent wettability on Mo and Nb substrates, especially upon increasing the test temperature from 900 to 950 °C. The addition of minor titanium into the Ag–Cu braze alloys can significantly improve its wettability on both substrates.
2. The brazed Mo/63Ag–35.25Cu–1.75Ti/Nb joint primarily consists of Ag-rich and Cu-rich phases. Because the Ti is completely miscible with Mo and Nb, there is no reaction product at the interface among the braze alloy and two substrates. From the viewpoint of brazing technology, it is preferred that the brazed joint is free of any brittle intermetallic compound. Accordingly, dimple-dominated fracture is extensively observed in the brazed joint.
3. The brazed Mo/68.8Ag–26.7Cu–4.5Ti/Nb joint primarily consists of Ag-rich, Cu-rich and Nb-rich phases. A few Cu–Ti intermetallics are found in the brazed joint due to higher Ti content in the braze alloy. However, the growth of Cu–Ti intermetallics is not prominent during brazing due to depletion of Ti content from the molten braze. Accordingly, the presence of Cu–Ti intermetallic phase demonstrates little effect on the shear strength of the brazed joint. Dimple-dominated fracture is observed for the 900 °C brazed joint.
4. The Nb-rich phase is found in both brazed joint, and its amount is increased with increasing brazing temperature and/or time. Therefore, the growth of the Nb-rich phase is greatly inhibited if the rapid infrared brazing is applied. The coarsening of the Nb-rich phase significantly deteriorates the shear strength of the brazed Mo/68.8Ag–26.7Cu–4.5Ti/Nb joint, and finally results in cleavage fracture of the joint.

#### Acknowledgements

The authors gratefully acknowledge the financial support of this research by the National Science Council (NSC), Republic of China under NSC grant 92-2216-E-259-001. EPMA analyses by Mr. H.D. Wang in NSC Instrument Center, National Sun Yat-Sen University, Kaohsiung, Taiwan, are also appreciated.

## References

- [1] W.F. Smith, Structure and Properties of Engineering Alloys, McGraw-Hill, New York, 1993, p. 571.
- [2] J.R. Davis (Ed.), Metals Handbook, vol. 2, Properties and Selection: Nonferrous Alloys and Special Purpose Materials, ASM International, Materials Park, OH, 1990.
- [3] M.M. Schwartz, Brazing, ASM International, Metals Park, OH, 1987, p. 77.
- [4] D.L. Olson, T.A. Siewert, S. Liu, G.R. Edwards (Eds.), ASM Handbook, vol. 6, Welding, Brazing and Soldering, ASM International, Materials Park, OH, 1993.
- [5] M. Schwartz, Brazing: For the Engineering Technologist, ASM International, Materials Park, OH, 1995.
- [6] G. Humpston, D.M. Jacobson, Principles of Soldering and Brazing, ASM International, Materials Park, OH, 1993.
- [7] N. Lashko, S. Lashko, Brazing and Soldering of Metals, MIR Publishers, Moscow, 1979.
- [8] Y. Hiraoka, Int. J. Refract. Met. H 11 (1992) 303.
- [9] Y. Hiraoka, Int. J. Refract. Met. H 11 (1992) 89.
- [10] Y. Hiraoka, S. Nishikawa, Int. J. Refract. Met. H 14 (1996) 311.
- [11] H.Y. Chan, D.W. Liaw, R.K. Shiue, Int. J. Refract. Met. H 22 (2004) 27.
- [12] H.Y. Chan, D.W. Liaw, R.K. Shiue, Mater. Lett. 58 (2004) 1141.
- [13] H.Y. Chan, R.K. Shiue, J. Mater. Sci. Lett. 22 (2003) 1659.
- [14] Y.L. Lee, R.K. Shiue, S.K. Wu, Intermetallics 11 (2003) 187.
- [15] R.K. Shiue, S.K. Wu, C.M. Hung, Metall. Mater. Trans. 33A (2002) 1765.
- [16] T.Y. Yang, S.K. Wu, R.K. Shiue, Intermetallics 9 (2001) 341.
- [17] R.K. Shiue, S.K. Wu, S.Y. Chen, Acta Mater. 51 (2003) 1991.
- [18] C.L. Ou, R.K. Shiue, J. Mater. Sci. 38 (2003) 2337.
- [19] C.C. Liu, C.L. Ou, R.K. Shiue, J. Mater. Sci. 37 (2002) 2225.
- [20] T.B. Massalski, Binary Alloy Phase Diagrams, ASM International, Materials Park, OH, 1990.
- [21] P. Villars, A. Prince, H. Okamoto, Handbook of Ternary Alloy Phase Diagrams, ASM International, Materials Park, OH, 1995.
- [22] R.K. Shiue, S.K. Wu, C.H. Chan, J. Alloy. Compd. 372 (2004) 148.